RSC Advances

ROYAL SOCIETY OF CHEMISTRY

www.rsc.org/advances

Synthesis and adsorption application of amine shield-introduced-released porous chitosan hydrogel beads for removal of Acid Orange 7 from aqueous solutions

Tingting Li[a,b], Yunguo Liu[a,b*], Shufan Wang[a,b], Guangming Zeng[a,b], Bohong Zheng[c], Hui Wang[a,b], Mingming Zhang[a,b], Fangying Guo[a,b], Xiaoxia Zeng[a,b]

[a] College of Environmental Science and Engineering, Hunan University, Changsha 410082, PR China

[b] Key Laboratory of Environmental Biology and Pollution Control (Hunan University), Ministry of Education, Changsha 410082, PR China

[c] School of Architecture and Art, Central South University, Changsha 410082, PR China

Abstract

An effective and low-cost adsorbent named amine shield-introduced-released porous chitosan hydrogel beads (APCB) was synthesized and characterized by SEM, EDX, FTIR, XPS and Zeta potential. SEM images showed the porous structure of APCB and EDX analysis proved the adsorption behavior of Acid Orange 7 (AO7)

* Corresponding author: Yun-guo Liu; Tel.: + 86 731 88649208; Fax: + 86 731 88822829;

E-mail address: yunguoliu12@163.com

onto APCB. FTIR analysis indicated that the amine-shield-release process and amine-introduce process both increased the amount of amine groups. XPS analysis confirmed the chemical compositions of the APCB. Zeta potential analysis indicated that the pH_{pzc} of APCB was 5.4. The significance of this work was illustrated by excellent adsorption capacity towards AO7. The maximum adsorption was observed at pH 2.0 with the adsorption capacity of 2803.77 mg g^{-1}. APCB showed low adsorption capacity in high pH values and exhibited better AO7 adsorption capacity in low ionic strength solutions. Experimental data were well fitted by pseudo-second-order kinetic model and Langmuir isotherm model. Thermodynamic analysis indicated that the adsorption process was spontaneous and endothermic.

Keywords: amine-shield chitosan; amine-introduce; acid orange 7 removal; adsorption

1. Introduction

Acid orange 7 (AO7) is an azo dye which is used in many industries, such as organic light-emitting diodes, textiles, hair dyes, leather materials, cosmetics, and foodstuffs [1]. The excessively release of dye introduces aesthetic concern and effects aquatic diversity by reducing the penetration of light [2]. Therefore, several technologies, like irradiation [3], reverse osmosis [4], ozonation [5] and adsorption [2], have been used to study the removal of hazardous dyes. Among these methods, adsorption is one of the most effective methods for dye removal because of simplicity in design,

low initial cost and easy operation. Researchers have exploited many natural materials as efficient adsorbents for their low cost, availability and biodegradability, such as zeolites, bottom ash and hen feathers [6].

Chitosan is a natural biopolymer produced by deacetylation of chitin [7]. Many forms of chitosan-based materials, such as nanoparticles [8], flakes or powder [9, 10], hydrogel [11], have been used to treat polluted wastewaters. Among these materials, chitosan hydrogel beads show enhanced adsorption capacity. And chitosan hydrogel beads are easy to regenerate after adsorption [12]. Chiou et al [13] have reported that AO7 could be absorbed by chemically cross-linked chitosan beads. Sheshmani [14] et al investigated the adsorption behavior of magnetic graphene/chitosan for AO7 in aqueous solution. However, hydrogel beads have large mass transfer resistance when the pollutant diffused [15]. In order to overcome this drawback, chitosan beads are usually prepared with porous structures. Porous chitosan beads provide a suitable adsorbing media for accessibility of dye, which can reduce the mass transfer resistances efficiently [16]. Favorable porous structures could be induced in the blend of chitosan by PEG (polyethylene glycol), because PEG can be dissolved when beads are washed with water. Then a lot of pores can be formed both on the surface and inside of the microspheres [15].

In the preparing of chitosan beads, cross-linking agent is usually used to improve the acid resistance of chitosan. However, cross-linking reaction is prone to react with the amine groups instead of the hydroxyl groups, which resulted in the reducing

number of amine groups on C2 position. Since the main chelating group on chitosan is amine group, the adsorption capacity is found to be effected by the number of amine groups in many researches [17]. To obtain more amine groups on the surface of chitosan, researchers have done many efficient works. For example, Hu [18] et al. found that the ethylenediamine-modified cross-linked magnetic chitosan resin improved Cr(VI) adsorption capacity. Dragan [19] et al. reported the enhanced sorption of Cu^{2+} by chitosan/poly(vinyl amine) composite beads. In this study, we proposed a novel chitosan-based adsorbent named amine shiled-intoduced-released porous chitosan beads (APCB), which was produced to enhance the acid orange 7 adsorption.

The main objectives of this manuscript were to: 1) prepare amine shiled-intoduced-released porous chitosan beads (APCB) and characterize it by SEM, EDX, FTIR, XPS and Zeta potenisal; 2) apply APCB as an adsorbent for decontamination of AO7 and evaluate the influences of adsorption conditions, i.e., pH, initial ion concentrations, temperature and ionic strength; 3) study the adsorption mechanism with kinetics, isotherm and thermodynamic models.

2. Materials and methods

2.1. Materials

Chitosan (85% deacetylated), formaldehyde (37%), glutaraldehyde (50%), polyethylene glycol (PEG 2000), epichlorohydrin and ethylenediamine were obtained

by Sinopharm Chemical Reagent Co., Ltd. AO7 was supplied by Xiya Reagent. All the chemicals were of analytical grade and deionized water was used to prepare all solutions.

2.2. Preparation of APCB

The synthesis of APCB had four main processes (the proposed scheme for the formation of APCB was shown in Fig. 1): 1) amine groups were shielded by formaldehyde before cross-linking reaction (step 1); 2) free amine groups were introduced on the activated hydroxyl groups (step 2 and 3); 3) the shielded amine were released after cross-linking (step 4); 4) poriferous structure was produced by using PEG as porogen.

3 g of chitosan was added into 100 mL of 1% (v/v) acetic acid to obtain a homogeneous solution. PEG was added into the chitosan solution and stirred to dissolve. The mixture was injected in droplets into 1% NaOH solution to form hydrogel beads and stay in the NaOH solution for 4 h. Then, the hydrogel beads were separated, washed and stored in 400 mL deionized water. After that, 5 mL formaldehyde was added and reacted at 40 °C for 2 h. Crosslinking reaction was worked by adding 5 mL glutaraldehyde at pH 9 by the addition of NaOH solution for 2 h [20, 21]. The amino-shield porous chitosan hydrogel beads (ASCB) were obtained by removing the water-soluble PEG in hot water (80–90 °C) [22].

The ASCB were then dispersed in 300 mL ethanol/water (v:v=1:1) solution and

epichlorohydrin was added to activate hydroxyl groups at pH 9, 60 °C for 2 h. Then, 13 mL ethylenediamine was added to introduce free amine groups. The mixture was reacted for 4 h and the beads were washed for further step. The shielded amine was then released by 0.5 M HCl. Finally, the APCB was obtained after washed by NaOH and deionized water. In addition, amino-introduced porous chitosan hydrogel beads (AICB) were prepared with the same process except the amine-shield and release step.

2.3. Characterization of APCB

The surface morphology of APCB was characterized with a scanning electron microscopy (SEM) (JSM–7001F, Japan) coupled with an energy dispersive X-ray (EDX) spectrometer (AMETER, USA). Function groups of adsorbents involved in the dye removal were examined by Fourier transform infrared spectrophotometer (FTIR） (Nicolet 5700 Spectrometer, USA). The elements of the samples were performed by an X–ray Photoelectron Spectrometer (XPS) (Thermo Fisher, USA). Surface potential of APCB and chitosan was determined by Zeta potential analyzer (ZEN3690, Malvern, UK.). The absorbance of the solution was analyzed with a UV-vis spectrophotometer (Pgeneral T6, Beijing) at a wavelength of 484 nm, which is the maximum absorption wavelength of AO7.

2.4. Dissolution and hydration rate test for APCB

The APCB was tested for the dissolution property and hydration rate. In the dissolution tests, APCB was placed in 0.1 M acetic acid, 0.1 M HCl, deionized water, or 0.1 M NaOH to observe their solubility. In the hydration tests, the APCB was taken out from the stock water and blotted up the surface water. After the beads weighed, the beads were placed into a vacuum desiccator at 40 °C for 48 h for drying. The weights of the dried beads were weighed again. The percentage of hydration was calculated by:

$$\text{Hydration rate} = \frac{W_{\text{wet}} - W_{\text{dry}}}{W_{\text{wet}}} \times 100\% \quad (1)$$

where W_{wet} is the weight of the hydrated beads weighed before the drying (g) and W_{dry} is the weight of dehydrated beads after the drying in the vacuum desiccator (g).

2.5. Adsorption experiments

All the adsorption experiments were performed as follows: 0.3 g of wet APCB was added to 50 mL AO7 solution in flasks. Initial solution pH was adjusted by HNO_3 or NaOH. Flasks were shaken at 150 rpm at the needed temperature.

For the effect of pH and ionic strength, the experiments (at pH 2.0 to 12.0, 30 °C and initial AO7 solution of 400 mg L^{-1}) were adjusted by different concentrations of NaCl (0, 0.002, 0.02, 0.2 mol L^{-1}). Kinetic experiments were carried out at 30 °C with 400 mg L^{-1} AO7 solution. Adsorption isotherms and thermodynamic data were

obtained at 15, 30 and 45 °C, with varied initial concentrations (20–4000 mg L^{-1}). All the experiments were carried out in triplicate parallel groups and the averages dates were recorded. Adsorption capacity of APCB for AO7 was calculated by the following equation:

$$q_e = \frac{(C_0 - C_e)V}{W_{wet} \times (1 - \text{hydration rate})} \quad (2)$$

where q_e is the equilibrium adsorption capacity (mg g^{-1}), C_0 and C_e are the initial and equilibrium concentration in the solution (mg L^{-1}), W_{wet} is the weight of the wet APCB, V is the volume of AO7 solution (L).

3 Results and discussion

3.1. Characteristics of adsorbents

3.1.1. SEM and EDX analysis

The morphology of APCB was observed with a relatively smooth and dense surface (Fig. 2a) and porous interior (Fig. 2b). As shown in Fig. 2b, numerous pores were formed on the APCB beads and two kinds of pores can be clearly observed. The larger one may be formed by the sublimation of ice crystals under vacuum, while the small one may be due to the dissolving of water-soluble PEG. After adsorption of AO7, the interior structure was obviously changed. It can be seen from Fig. 2c and Fig. 2d that the poriferous structure became rough due to the accumulation of the large amount of AO7.

The EDX analysis was further tested to study the difference of surface chemical compositions before and after adsorption. Compared with Fig. 2e, Fig. 2f showed that the peak of S was appeared after AO7 adsorption, which provided a directly evidence of the existence of AO7.

3.1.2. FTIR analysis

To better understand the changes after amine was shielded and introduced, FTIR spectroscopy was conducted on amine shield-introduced-released porous chitosan hydrogel beads (APCB), amino-shield porous chitosan hydrogel beads (ASCB) and amino-introduced porous chitosan hydrogel beads (AICB). As is seen from Fig. 3a, the main peaks of APCB are OH/NH stretching vibration (at 3417 cm^{-1}), C–H stretch vibrations of –CH and $–CH_2$ (2869 cm^{-1}), $–NH_2$ (1665 cm^{-1}), coupling of C-N/N-H and C=N (1446 cm^{-1}), –CN stretching vibration (1067 cm^{-1}) and C–O stretching vibration (1021 cm^{-1}) [23-26]. Comparing the FTIR spectra of APCB and ASCB, peaks of some nitrogen-containing groups on APCB, such as the peaks at 3417 cm^{-1} (OH/NH), 1665 cm^{-1} (NH_2), 1446 cm^{-1} (C–N/N–H) and 1067 cm^{-1} (CN), are obviously sharpened, indicating the successfully introduction of new amine groups. The increased intensity of C–O peak of APCB may be due to epichlorohydrin (used to activate the –OH). The bands of AICB at 3417 cm^{-1}, 1665 cm^{-1} and 1067 cm^{-1} are weaker than that of APCB, indicating that more NH_2 groups were generated on the APCB than on the AICB. In other words, amine groups were preserved successfully

by amine-shield-released process. This is because that the C=N groups (formed in the formaldehyde shield process) converted back into the $-NH_2$ groups by the HCl treatment (as shown in Eq(3)) [17]. From the discussions above, both the amine-shield-release process and the amine introduce process can increase the number of the NH_2 groups successfully.

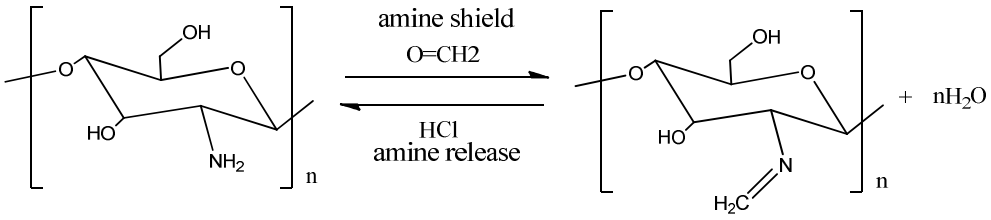

(3)

FTIR spectra for the AO7 and APCB (before and after adsorption) are shown in Fig. 3b. As for the spectra of AO7, the peak at 1622 cm^{-1}, 1600-1450 cm^{-1}, 1215 cm^{-1} are assigned to the C=N stretching C=C stretching and N-N stretching vibrations, respectively. The bands at 1123 cm^{-1} and 1037 cm^{-1} are due to the coupling between the benzene mode and *vs*(SO_3) [27, 28]. After the adsorption of AO7, main bands of AO7 can be observed clearly on the spectra of AO7-APCB, which attributed to the exceptional adsorption properties of APCB towards AO7. Moreover, almost all the characteristic peaks of APCB are weakened and even disappeared, demonstrating that NH_2 groups and OH groups were involved during the AO7 adsorption.

3.1.3. XPS analysis

The XPS analysis was used to study the surface chemical compositions of the APCB. The wide scan XPS spectrum (Fig. 4a) of APCB shows photoelectron lines at

binding energies of about 284.6 eV, 399.8 eV and 533.3 eV which are attributed to C1s, N1s and O1s, respectively. The principal elements at the surface of the APCB are carbon (61.9%), oxygen (29.75%), nitrogen (8.37%). The C1s XPS spectrum for the APCB (Fig. 4b) can be well fitted into three peak components at 284.6 eV (C−C), 285.7 eV (C−N), 287.2 eV (C−NH_2) [29]. The N1s spectrum of APCB (Fig. 4c) can be curve-fitted into three binding energy peaks at 398.7 eV, 399.7 eV and 401.1 eV, which attribute to the C-NH_2, C-N and protonated nitrogen atoms in the amine groups [30-32]. These results also agree with the EDX analysis and FTIR analysis.

3.1.4. Zeta potential, Hydration and solubility properties

The zeta potential were measured and presented in Fig. 5a. As can be seen, both APCB and chitosan have positive zeta potentials in acidic conditions but negative zeta potentials in basic solutions. The pH_{PZC} of APCB and chitosan was found at 5.4 and 6.3, respectively. From the electrostatic interaction point of view, the adsorption of AO7 anions on the adsorbents may be improved with the decrease of solution pH, due to the increase of the attractive surface electrostatic interactions.

In the solubility properties test, the APCB could not be dissolved in the test solutions, indicating that APCB possesses a good stability in acid and basic solutions. This is because of the crosslinking reaction, which extended the chemical stability of the hydrogel beads [33]. Furthermore, the hydration rate of APCB was 94.2%.

3.2. Effect of solution pH

The comparison of adsorption capacity between APCB and chitosan was performed by varying the initial pH from 2.0 to 12.0. As observed in Fig. 5b, the adsorption capacity of APCB ranged from 1116.98 mg g^{-1} to 49.41 mg g^{-1} while the chitosan ranged from 980.48 mg g^{-1} to 0 mg g^{-1}, respectively. The adsorption capacity of APCB was 1.1 to 13 times higher than that of chitosan. Based on the results in Fig.5b, the pH effect on the AO7 adsorption was significant. The adsorption capacity increased as the solution pH ranged from 12.0 to 2.0, and reached the maximum adsorption amount at the pH of 2.0. This was due to the solution pH affected the adsorption mechanism between adsorbents and dye anions.

At pH 2.0–3.0, AO7 was adsorbed mainly by electrostatic attractions. As the pH_{PZC} of APCB and chitosan are 5.4 and 6.3, the AO7 anions will promote a stronger coulombic attraction towards the protonated $–NH_2$ of APCB and chitosan. Therefore, the adsorption capacity of APCB and chitosan for AO7 was both high at low pH. Although chitosan possessed a more positive zeta potential than APCB, the adsorption capacity of chitosan was lower than APCB. This may because that the electrostatic attraction was not the only mechanism in AO7 removal process. The hypothetical mode of AO7 adsorption on APCB, as shown in Fig. 6, may involved both electrostatic interaction and hydrogen bonding. The aromatic rings, hydroxyl, the nitrogen atoms and the sulfonate from AO7 may form hydrogen bonds with oxygen

containing groups on the APCB surface [34]. It is also noteworthy that the bad acid resistance of chitosan made it hard to be separated after adsorption. APCB overcome this drawback because of its excellent acid resistance and physical size. With the increasing of pH, the electrostatic attraction diminished, which resulted in a rapid decrease of adsorption capacity. Moreover, at alkaline solutions, the surface of adsorbents became negatively charged, leading to the competition between OH^- and dye anions. The dramatically higher adsorption capacity of APCB towards chitosan may be due to its great number of $–NH_2$ and the highly porous structure. Given the aforementioned discussion, the initial solution pH 2.0 and 4.0 were used for the further experiments, because 2.0 is the optimum pH while 4.0 is close to the current value in industrial AO7 dye effluents [35].

3.3. Effect of ionic strength

The effect of ionic strength on the adsorption of AO7 on APCB was studied and the result is shown in Fig. 5c. As seen from Fig. 5c, the adsorption capacity of APCB decreased as the NaCl concentration ranked from 0 to 0.2 M. Generally, three reasons should be responsible for this phenomenon. Firstly, the high ionic strength of the solution influenced the activity coefficient of anions, leading to great decrease of the collide and contact between the sorbent and AO7 [36]. Secondly, the competition of Cl^- with dye anions for the adsorption sites results in the decrease of the uptake capacity. Finally, the screening effect was enhanced with the increase of NaCl concentration,

thus the adsorption capacity decreased.

3.4. Adsorption kinetics

Adsorption kinetics is an important parameter in understanding the process of adsorption [37]. Pseudo-first-order (Eq. (4)) and pseudo-second-order (Eq. (5)) models were applied to fit the experimental data to predict the corresponding adsorption kinetics.

The equations are generally expressed as follows:

$$q_t = q_e(1 - e^{(-k_1 t)}) \quad (4)$$

$$q_t = \frac{q_e^2 k_2 t}{1 + q_{e,2} k_2 t} \quad (5)$$

where q_e and q_t (mg g^{-1}) represented the sorption amount of AO7 at equilibrium and at time t, k_1 (min^{-1}) and k_2 (g mg^{-1} min^{-1}) are the pseudo-first-order and pseudo-second-order reacted rate constant, respectively.

The effect of contact time on AO7 adsorption by the APCB was represented in Fig. 7a. The correlation coefficients (shown in Table 1) of pseudo-second-order (0.99, 0.95) are higher than those of pseudo-first-order (0.97, 0.89). The value of q_e (1192.70 mg g^{-1}, 439.99 mg g^{-1}) calculated from pseudo-second-order model was more agreeable to the experimental (1146.50 mg g^{-1}, 463.42 mg g^{-1}) value. Therefore, the AO7 adsorption process complied with the second-order type kinetic reaction. The good fit of the data to this model implied that the rate-limiting step of AO7 adsorption was due to the

chemisorptions, where valency forces were involved via electrons sharing or exchange between the APCB and AO7 [38]. Jin [27] et al. reported similar result with the AO7 adsorption onto surfactant-coated zeolite. Moreover, a longer time (16h) at pH 4 was needed to reach the sorption equilibrium than that of pH 2 (8h). This was also proved by the k_2 in Table 1. [39].

To identify the diffusion of sorption process, regression analysis was further carried out by using the intraparticle diffusion model, which can be described as follows:

$$q_t = k_i t^{0.5} + C \quad (6)$$

where k_i is the intraparticle diffusion rate constant (mg (g $min^{-0.5}$)$^{-1}$), C is the intercept, the intraparticle diffusion was the only rate-limiting step when the linear passes through the origin [40].

The plots of intraparticle diffusion model are shown in Fig. 7b. As can be seen, the plots present multilinearity, indicating the overall adsorption process was divided into three stages. It occurs because of the change in diffusion driving force which is strongly dependent on the availability of dye per unit mass of adsorbent [40]. The trend was also found in many adsorption processes [40, 41]. From Fig. 7b, we can see that 71.55% of the AO7 was adsorbed at pH 2.0 during the external mass transfer region, while only 30.45% was adsorbed at pH 4.0. This was because that the removed AO7 at external mass transfer process owed to the protonated amine groups on the outer surface of APCB. After the external mass transfer region, the adsorption process

turned into gradual adsorption stages, where the intra-particle diffusion was rate-controlling step. Finally, all the active sites of APCB were occupied by the dye molecules. The intra-particle diffusion rate started to slow down and saturation adsorption began.

3.5. Adsorption isotherms and thermodynamics

The equilibrium adsorption isotherms provide information about the surface properties of adsorbent and the adsorption behavior, while thermodynamic parameters provide in-depth information about the feasibility and exothermic nature of the adsorption process [29]. Langmuir (Eq. (7)) and Freundlich (Eq. (8)) isotherm models and thermodynamic parameters (Eq. (9, 10)) are simulated by the following equations:

$$q_e = \frac{q_m K_L C_e}{1 + K_L C_e} \quad (7)$$

$$q_e = K_F C_e^{1/n} \quad (8)$$

$$\ln k_e = -\frac{\Delta H^0}{RT} + \frac{\Delta S^0}{R} \quad (9)$$

$$\Delta G^0 = -RT \ln k_e \quad (10)$$

where q_e (mg g^{-1}) is the adsorption capacity at equilibrium concentration, q_m (mg g^{-1}) is the maximum adsorption capacity, C_e (mg L^{-1}) is the equilibrium concentration of AO7. K_L (L mg^{-1}) is the Langmuir affinity constant. K_F and n are the Freundlich constants, respectively. T (K) is the absolute temperature, ΔS^0 (kJ mol^{-1} k^{-1}) is the entropy change, ΔH^0 (kJ mol^{-1}) is the enthalpy change, k_0 was calculated by plotting

ln K (K=q_e/C_e) versus C_e and extrapolating C_e to zero.

The Langmuir and Freundlich adsorption isotherms are shown in Fig. 7c and Fig. 7d, and the related parameters are listed in Table 2. It could be obviously observed that R^2 values of Langmuir model (0.91–0.98) were generally better than those of Freundlich model (0.80–0.97). Therefore, Langmuir model was more suitable for the adsorption process, indicating that monolayer coverage of APCB was the main adsorption mechanism [38]. From Table 2, the values of q_m at 15, 30 and 45 ℃ were 2499.30, 2570.95 and 2803.77 mg g^{-1} at pH 2.0, while 333.35, 363.57 and 409.32 mg g^{-1} at pH 4.0. The higher adsorption amount of APCB at pH 2.0 was agreed with prediction in zeta potential section. Moreover, both q_m and K_L of the Langmuir model increased with the rise of temperature, which indicated the endothermic adsorption process of AO7 onto APCB [38]. These results were coincident with the positive ΔH^0 values obtained from the inset of Fig. 7c and 7d. Moreover, the positive value of ΔS^0 indicated an increasing randomness at the solution interface during the adsorption. Furthermore, all the ΔG^0 values in Table 3 are negative, indicating the adsorption process was feasibility and spontaneous. The obtained ΔG^0 values at pH 2 were more negative than that of pH 4, indicating a more favorable adsorption process at low pH value.

3.6. Comparison of AO7 adsorption of various adsorbents

The maximum adsorption capacity of APCB for the removal of AO7 was

compared with those documented in the literature to illustrate the significance of this work [13, 42-44]. From Table 4, APCB showed extraordinary AO7 adsorption capacities (2803.77 mg g^{-1}) compared with other adsorbents, like activated carbon, zeolite, titania, sludge and some chitosan-based materials. Moreover, there are other advantages of APCB, such as easy availability, non-toxicity and lower cost in production. Therefore, APCB is expected to be an inexpensive and highly efficient adsorbent for AO7 polluted water in the further.

4. Conclousion

In this study, the amine shield-introduced-released porous chitosan hydrogel beads (APCB) was successfully synthesized to remove acid orange 7 (AO7) from the wastewater. The porous structure of APCB was obvious observed from the SEM images. The EDX analysis revealed the directly evidence that AO7 can be successful adsorbed by APCB. FTIR and XPS analysis indicated that the $–NH_2$ groups on the chitosan were successfully shielded by formaldehyde and converted back to amine groups under the treatment of HCl. In addition, new amine groups were also favorably introduced.

The adsorption capacity of APCB was influenced by the solution pH and the maximum adsorption amount was found at the pH 2.0. The presence of NaCl in the solution had a negative influence in the adsorption process. The experimental data was well fitted by the pseudo-second-order and Langmuir models. The APCB showed

excellent AO7 adsorption capacities (2803.77 mg g^{-1}) compared with other adsorbents. The thermodynamic study revealed the spontaneity and endothermic natures of AO7 adsorption. Results obtained from this study showed that APCB is an effective and inexpensive adsorbent for AO7 polluted water.

Acknowledgements

The authors would like to thank financial support from the National Natural Science Foundation of China (Grant No. 41271332 and 51478470).

References

1. M. Yun, J. E. Choe, J. M. You, M. S. Ahmed, K. Lee, Z. Ustundag and S. Jeon, *Food chem.*, 2015, 169, 114-119.
2. T. S. Anirudhan and M. Ramachandran, *Process Saf. Environ. Prot.*, 2015, 95, 215-225.
3. V. Vaiano, O. Sacco, D. Sannino and P. Ciambelli, *Appl. Catal., B*, 2015, 170-171, 153-161.
4. S. K. Nataraj, K. M. Hosamani and T. M. Aminabhavi, *Desalination*, 2009, 249, 12-17.
5. A. Manivel, G.-J. Lee, C.-Y. Chen, J.-H. Chen, S.-H. Ma, T.-L. Horng and J. J. Wu, *Mater. Res. Bull.*, 2015, 62, 184-191.
6. A. Mittal, V. Thakur and V. Gajbe, *Environ Sci. Pollut. Res. Int.,* 2013, 20, 260-269.
7. Q.-Q. Zhong, Q.-Y. Yue, B.-Y. Gao, Q. Li and X. Xu, *Chem. Eng. J.,*2013, 229, 90-98.
8. M. Ziegler-Borowska, D. Chełminiak, T. Siódmiak, A. Sikora, M. Piotr Marszałł and H. Kaczmarek, *Mater. Lett.*, 2014, 132, 63-65.
9. R. Karthik and S. Meenakshi, *Chem. Eng. J.*, 2015, 263, 168-177.
10. G. Z. Kyzas, P. I. Siafaka, E. G. Pavlidou, K. J. Chrissafis and D. N. Bikiaris, *Chem. Eng. J*, 2015, 259, 438-448.

11. J. A. Silva, G. P. Macedo, D. S. Rodrigues, R. L. C. Giordano and L. R. B. Gonçalves, *Biochem. Eng. J.*, 2012, 15, 16-24.
12. N. Li and R. Bai, *Ind. Eng. Chem. Res.*, 2005, 44, 6692-6700.
13. M. Chiou, P. Ho and H. Li, *Dyes and Pigments*, 2004, 60, 69-84.
14. S. Sheshmani, A. Ashori and S. Hasanzadeh, *Int J Biol Macromol*, 2014, 68, 218-224.
15. H. Zhao, J. Xu, W. Lan, T. Wang and G. Luo, Chem. Eng. J, 2013, 229, 82-89.
16. E. Salehi and S. S. Madaeni, *Appl. Surf. Sci.*, 2014, 288, 537-541.
17. N. Li and R. Bai, *Ind. Eng. Chem. Res.*, 2005, 44, 6692-6700.
18. X.-j. Hu, J.-s. Wang, Y.-g. Liu, X. Li, G.-m. Zeng, Z.-l. Bao, X.-x. Zeng, A.-w. Chen and F. Long, *J Hazard Mater.*, 2011, 185, 306-314.
19. E. S. Dragan, A. I. Cocarta and M. V. Dinu, *Chem. Eng. J*,, 2014, 255, 659-669.
20. S.-I. Park, I. S. Kwak, S. W. Won and Y.-S. Yun, *J Hazard Mater.*, 2013, 248-249, 211-218.
21. T. Li, Y. Liu, Q. Peng, X. Hu, T. Liao, H. Wang and M. Lu, *Chem. Eng. J,*, 2013, 214, 189-197.
22. M. Zeng, X. Zhang, L. Shao, C. Qi and X.-M. Zhang, *J. Organomet. Chem.*, 2012, 704, 29-37.
23. M. Monier, D. M. Ayad, Y. Wei and A. A. Sarhan, *React. Funct. Polym.*, 2010, 70, 257-266.
24. M. Zhang, Y. Zhang and R. Helleur, *Chem. Eng. J,*, 2015, 264, 56-65.

25. R. Mata, J. Reddy Nakkala and S. Rani Sadras, *Mater. Sci. Eng.*, 2015, 51, 216-225.

26. L. Huang, M. Zhai, J. Peng, L. Xu, J. Li and G. Wei, *J. colloid interf. Sci.*, 2007, 316, 398-404.

27. X. Jin, B. Yu, Z. Chen, J. M. Arocena and R. W. Thring, *J. colloid interf. Sci.*, 2014, 435, 15-20.

28. G. Zhang, J. Qu, H. Liu, A. T. Cooper and R. Wu, *Chemosphere*, 2007, 68, 1058-1066.

29. W. Xu, S. Wang, Y. Liu, G. Zeng, B. Zheng, X. Tan, T. Li, H. Wang, F. Guo and M. Zhang, *RSC Adv.*, 2015, 5, 24009-24015.

30. D. Gogoi, A. J. Choudhury and J. Chutia, *Appl. Surf. Sci.*, 2015, DOI: 10.1016/j.apsusc.2015.02.125.

31. S. Deng and R. Bai, *Water Res*, 2004, 38, 2423-2431.

32. M. Rong, L. Lin, X. Song, Y. Wang, Y. Zhong, J. Yan, Y. Feng, X. Zeng and X. Chen, Chen, *Biosens. Bioelectron.*, 2015, 68, 210-217.

33. N. Li and R. Bai, *Sep. Purif. Methods*, 2005, 42, 237-247.

34. L. Abramian and H. El-Rassy, *Chem. Eng. J*, 2009, 150, 403-410.

35. J. Pedro Silva, S. Sousa, J. Rodrigues, H. Antunes, J. J. Porter, I. Gonçalves and S. Ferreira-Dias, *Sep. Purif. Methods*, 2004, 40, 309-315.

36. C. Gan, Y. Liu, X. Tan, S. Wang, G. Zeng, B. Zheng, T. Li, Z. Jiang and W. Liu, *RSC Adv.*, 2015, 5, 35107-35115.

37. L. Fang, D. Yang, Z. Chen, M. Megharaj, R. Naidu, *J Hazard Mater.*, 2015, 296, 37-45.

38. H. Wang, Y. G. Liu, G. M. Zeng, X. J. Hu, X. Hu, T. T. Li, H. Y. Li, Y. Q. Wang and L. H. Jiang, *Carbohydr Polym*, 2014, 113, 166-173.

39. P. W, R. W and P. A, *Adv. Colloid Interface Sci.*, 2009, 152, 2-13.

40. D. Kumar and J. P. Gaur, *Bioresour. Technol.*, 2011, 102, 633-640.

41. T. S. Singh and K. K. Pant, *Sep. Purif. Methods*, 2004, 36, 139-147.

42. E. Géraud, M. Bouhent, Z. Derriche, F. Leroux, V. Prévot and C. Forano, *J. Phys. Chemi. Solids*, 2007, 68, 818-823.

43. C. Hsiu-Mei, C. Ting-Chien, P. San-De and H. L. Chiang, *J Hazard Mater*, 2009, 161, 1384-1390.

44. B. Sarkar, Y. Xi, M. Megharaj and R. Naidu, *Appl. Clay Sci.*, 2011, 51, 370-374.

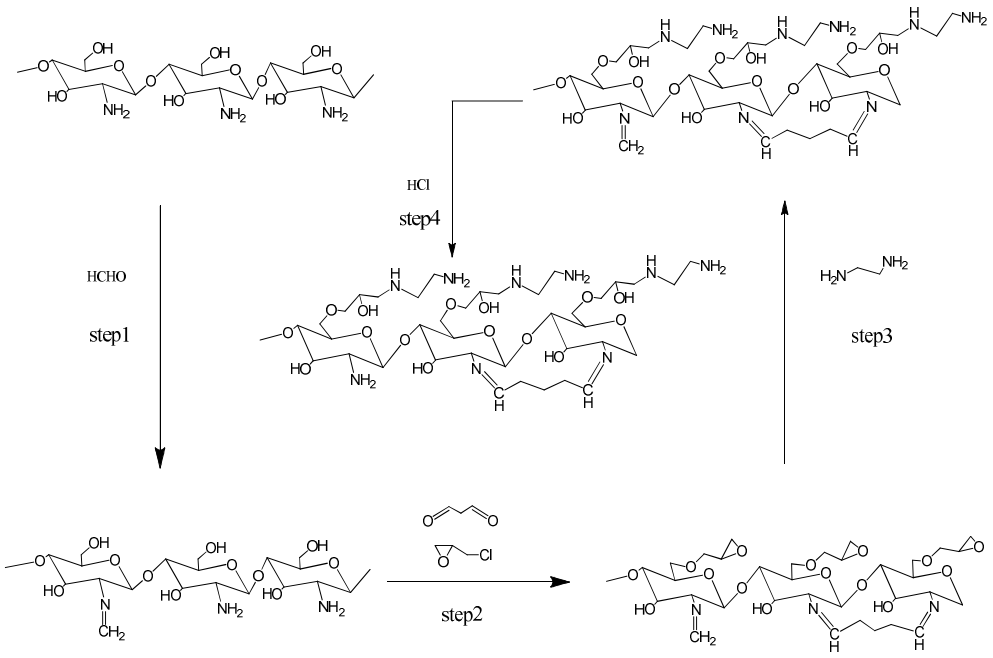

Fig.1. The proposed scheme for the formation of APCB.

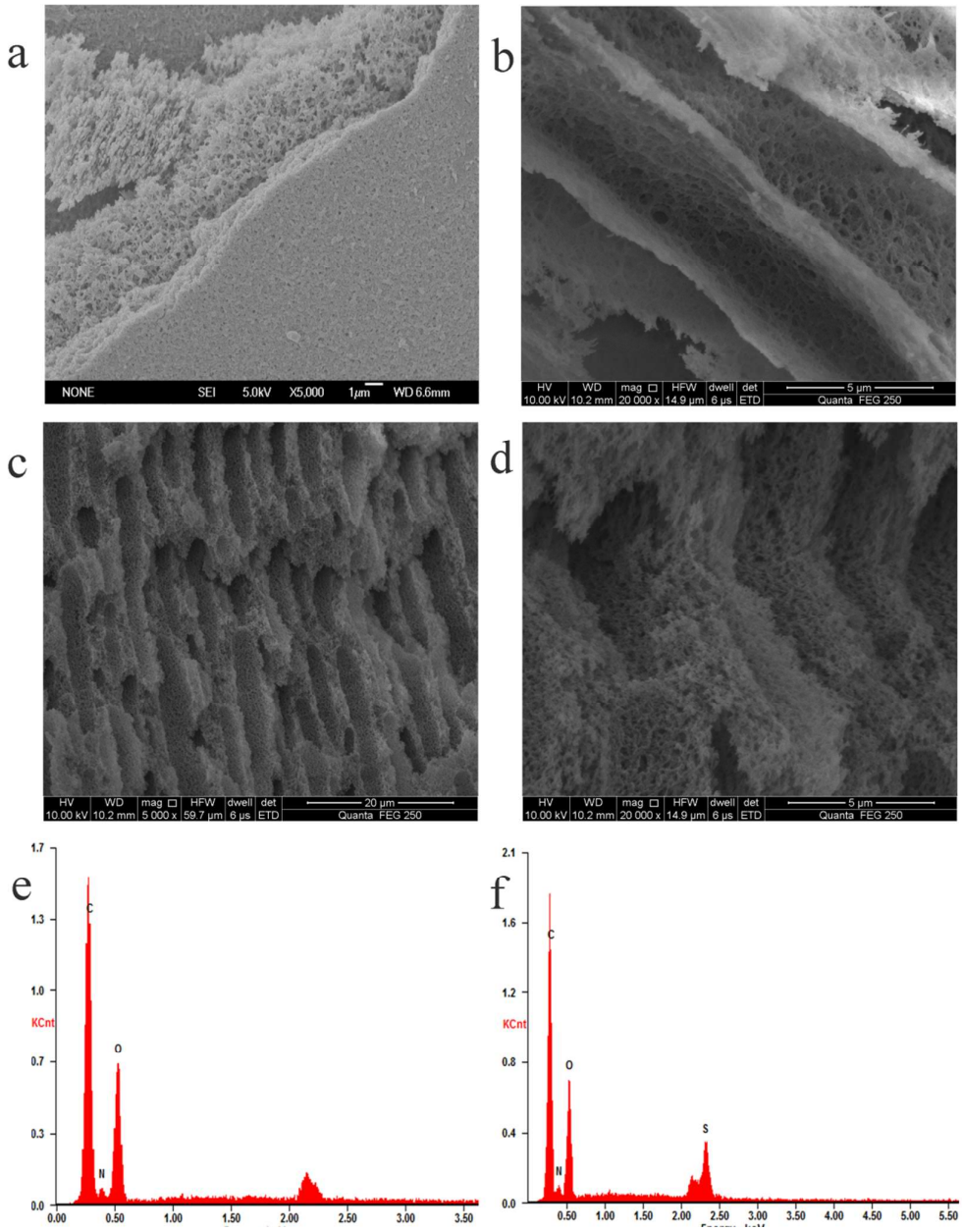

Fig. 2. (a) and (b) SEM images of APCB; (c) and (d) SEM images of APCB after adsorption; (e) EDX result of APCB and (f) EDX result of APCB after adsorption.

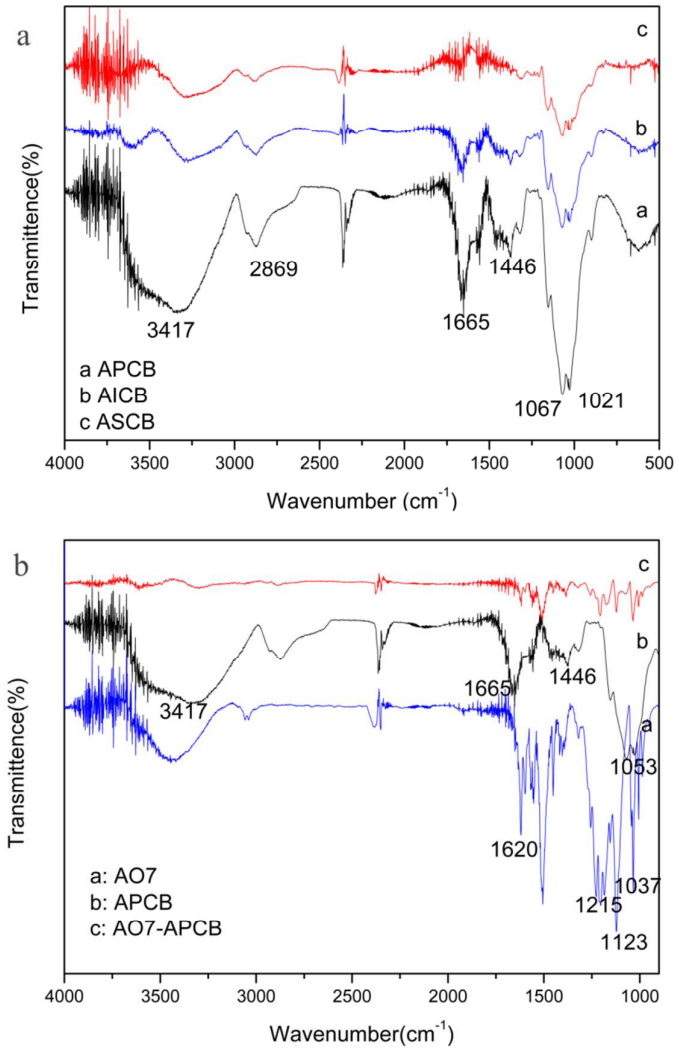

Fig. 3. (a) FTIR spectra of APCB, amino-shield porous chitosan hydrogel beads (ASCB) and amino-introduced porous chitosan hydrogel beads (AICB); (b) FTIR spectra of AO7, APCB and APCB after adsorped AO7 (AO7-APCB).

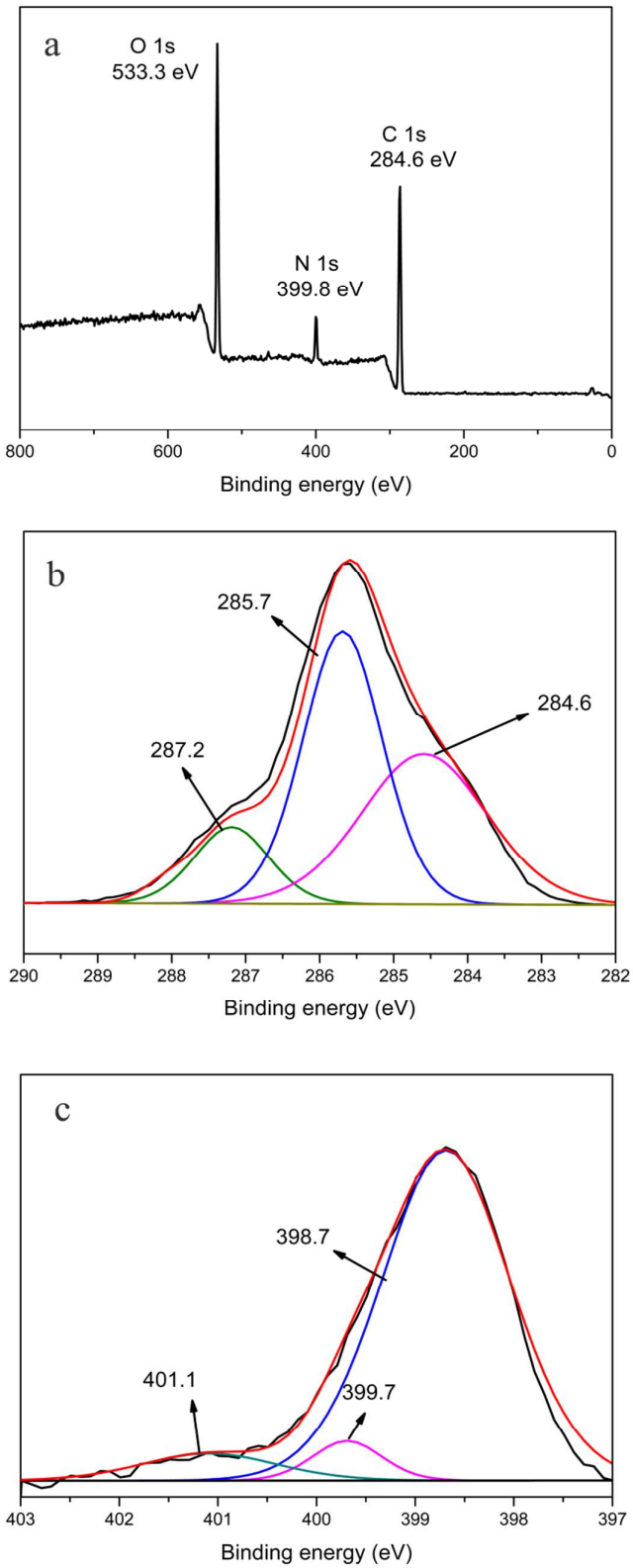

Fig. 4. (a) XPS wide-scan of APCB; (b) C1s XPS spectra of APCB; (c) N1s XPS spectra of APCB.

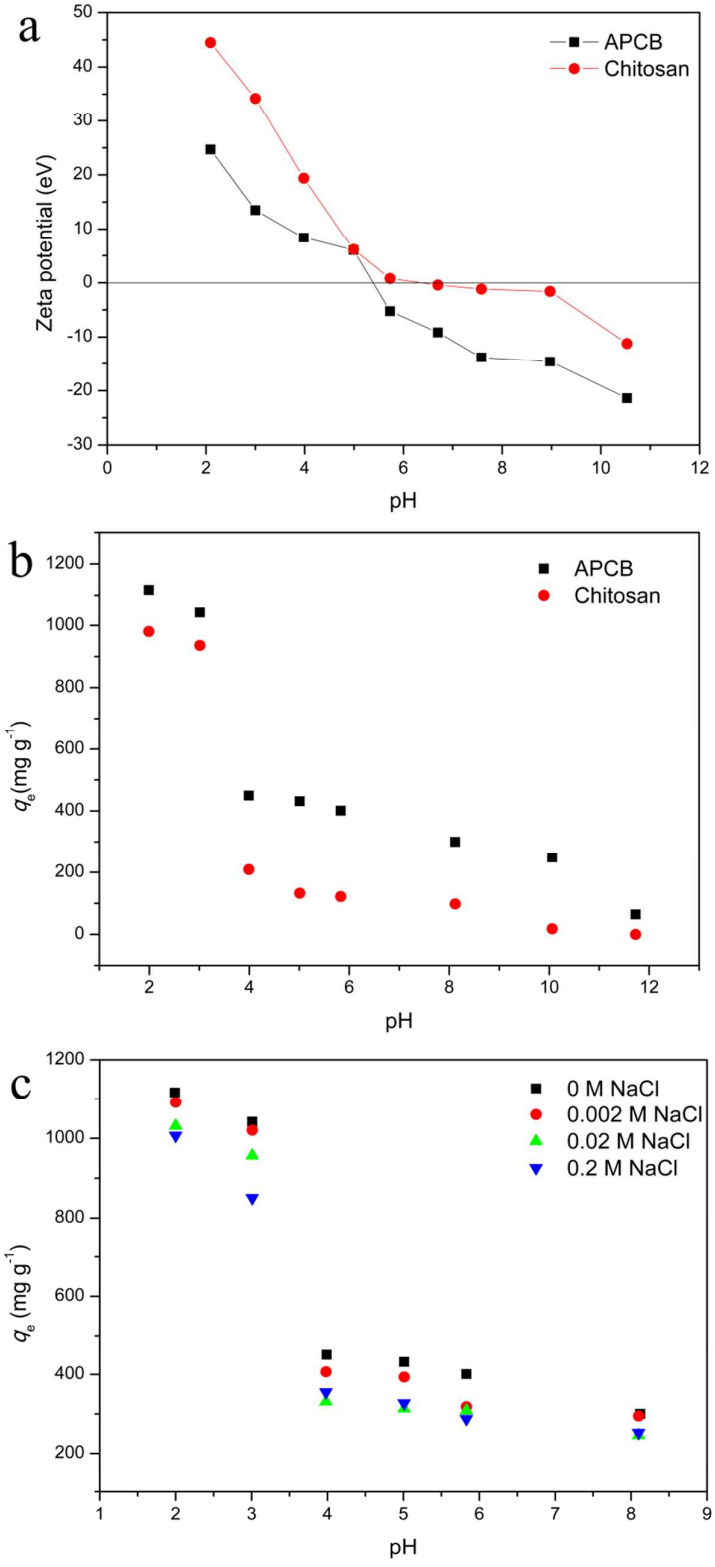

Fig.5. (a) Zeta potential of APCB and chitosan; (b) effect of pH on AO7 adsorption by APCB and chitosan; (c) Effect of ionic strength on AO7adsorption by APCB.

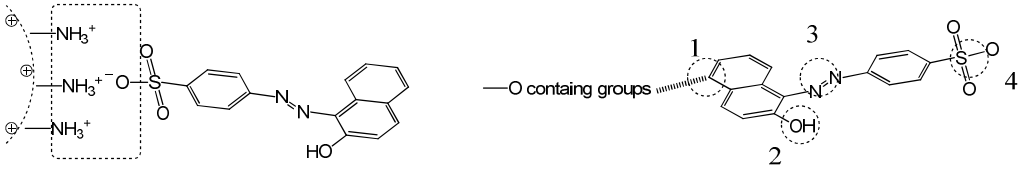

electrostatic attraction hydrogen bonding

Fig. 6. The hypothetical mode of AO7 adsorption on APCB. (the rectangle in the left represents electrostatic attraction between the protonated $–NH_2$ and AO7 anions; the round in the right represents the hydrogen bonding position, 1 aromatic rings, 2 hydroxyl, 3 nitrogen atoms and 4 sulfonate.)

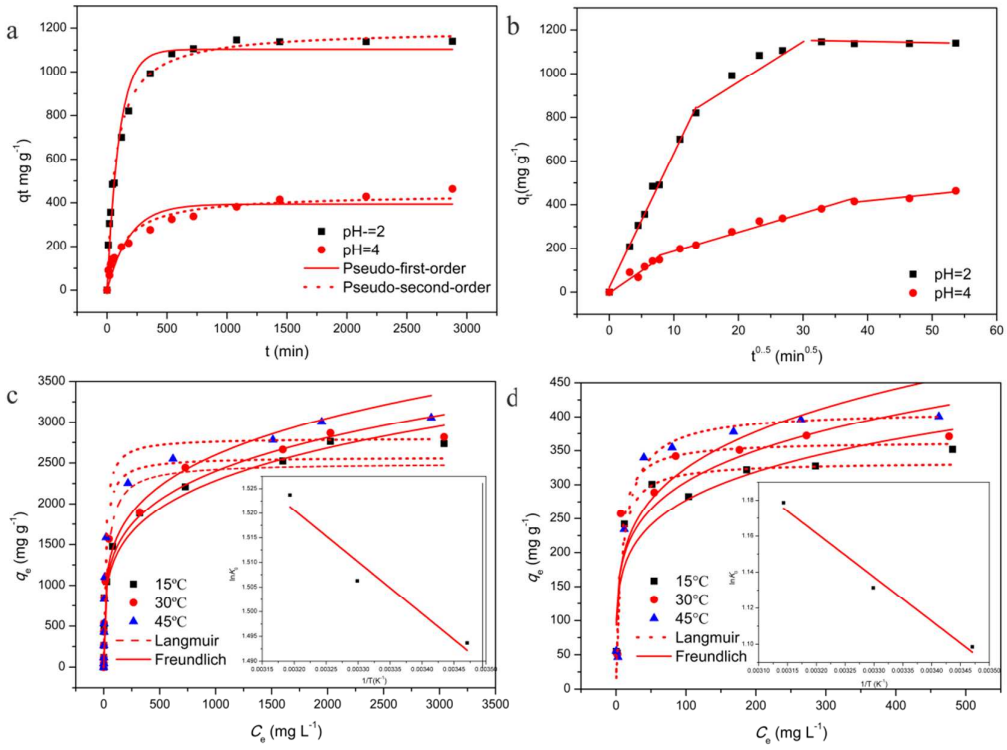

Fig. 7. (a) Pseudo-first-order and Pseudo-second-order kinetic models at pH 2 and 4; (b) intraparticle diffusion kinetic model at pH 2 and 4; (c) Langmuir and Freundlich adsorption isotherms at pH 2 (the inset show the plot $\ln K^0$ versus $1/T$ for estimation of thermodynamic parameters); (d) Langmuir and Freundlich adsorption isotherms at pH 4 (the inset show the plot $\ln K^0$ versus $1/T$ for estimation of thermodynamic parameters).

Table 1. Kinetic parameters for adsorption of AO7 on APCB

pH	$q_{e,exp}$ (mg g^{-1})	Pseudo-second-order			Pseudo-first-order		
		q_e (mg g^{-1})	k_1(min^{-1})	R^2	q_e (g mg^{-1})	k_2(min^{-1})	R^2
2	1140.30	1192.70	1.16×10^{-5}	0.99	1103.42	1.0×10^{-2}	0.97
4	463.42	439.99	1.60×10^{-5}	0.95	394.04	5.0×10^{-3}	0.89

Table 2. Langmuir and Freundlich isotherm parameters for adsorption of AO7 on APCB

T(°C)	Langmuir model at pH 2			Freundlich model at pH 2		
	q_m(mg g^{-1})	K_L(L mg^{-1})	R^2	K_F(L mg^{-1})	n	R^2
15	2499.30	0.03	0.93	454.99	4.26	0.97
30	2570.95	0.05	0.95	493.77	4.37	0.96
45	2803.77	0.06	0.98	529.09	4.34	0.93
T(°C)	Langmuir model at pH 4			Freundlich model at pH 4		
	q_m(mg g^{-1})	K_L(L mg^{-1})	R^2	K_F(L mg^{-1})	n	R^2
15	333.35	0.17	0.96	109.01	4.94	0.83
30	363.57	0.19	0.91	119.16	4.92	0.80
45	409.32	0.09	0.97	116.49	4.50	0.82

Table 3. Thermodynamic parameters for adsorption of AO7 on APCB

pH	T(°C)	ΔG^0(kJ mol^{-1})	ΔS^0(J K^{-1} mol^{-1})	ΔH^0(kJ mol^{-1})	R^2
	15	-3.60			
2	30	-3.81	15.46	0.87	0.90
	45	-4.02			
	15	-2.42			
4	30	-2.85	16.13	2.03	0.97
	45	-3.12			

Table 4. Comparison of AO7 adsorption of various adsorbents.

Adsorbent	Adsorption capacity ($mg\ g^{-1}$)	Reference
APCB	2803.77	This study
Chemically cross-linked chitosan beads	1940	[13]
Calcined Macroporous hydrotalcite	1540	[42]
Activated carbon fibre prepared from pitch	1260	[43]
highly porous titania aerogel	420	[34]
Activated carbon	404	[28]
Sludge from biological waste water plant	350	[43]
ODTMA-palygorskite	99.01	[44]
hexadecyltrimethylammonium bromide-coated zeolite	38.96	[27]
Spent brewery grains	30.47	[35]